Infrared spectroscopic observation of the radical (XeF3)-Xe-center dot generated in solid argon

ARTICLE *in* INORGANIC CHEMISTRY · AUGUST 2009

Impact Factor: 4.76 · DOI: 10.1021/ic9007312 · Source: PubMed

4 AUTHORS, INCLUDING:

Eugenii Ya Misochko
Russian Academy of Sciences
65 PUBLICATIONS **527** CITATIONS
SEE PROFILE

Alexander Akimov
Russian Academy of Sciences
51 PUBLICATIONS **472** CITATIONS
SEE PROFILE

Daniil Tyurin
Lomonosov Moscow State University
42 PUBLICATIONS **266** CITATIONS
SEE PROFILE

Inorganic Chemistry
Article

Inorg. Chem. **2009**, *48*, 8723–8728 **8723**
DOI: 10.1021/ic9007312

Infrared spectroscopic observation of the radical $^{\bullet}XeF_3$ generated in solid argon

Eugenii Ya. Misochko,*,† Alexander V. Akimov,† Vasilii A. Belov,† and Daniil A. Tyurin‡

†*Institute of Problems of Chemical Physics of the Russian Academy of Sciences, 142432 Chernogolovka, Moscow Region, Russia, and* ‡*Department of Chemistry, Lomonosov Moscow State University, 119899, Moscow, Russia*

Received April 15, 2009

Xenon trifluoride radicals were generated by the solid-state chemical reaction of mobile fluorine atoms with XeF_2 molecules isolated in a solid argon matrix. On the basis of spectroscopic and kinetic FTIR measurements and performed quantum chemical calculations, two infrared absorption bands at 568 (strong) and 523 (very weak) cm^{-1} have been assigned to asymmetric and symmetric Xe−F stretching vibrational modes of radical $^{\bullet}XeF_3$, respectively. Chemical reaction of fluorine atom with XeF_2 in a solid argon cage obeys specific kinetic behavior indicating the formation of a long-lived intermediate complex under the condition that the diffusing fluorine atom is attached to isolated XeF_2 at temperatures 20 K < T < 27 K. Subsequent thermally activated conversion in the complex is the main source of novel xenon-containing radical species $^{\bullet}XeF_3$. The rate constant and energy barrier are estimated for the reaction in an argon cage, $[XeF_2{-}F]\rightarrow^{K_r}[XeF_3]$, as $K_r \sim 7\times10^{-5}$ c^{-1} at 27 K and $E \approx 1.2$ kcal/mol, respectively. Quantum chemistry calculations reveal that radical $^{\bullet}XeF_3$ has a planar C_{2v} structure. DFT calculations show that formation of the third Xe−F bond in the $^{\bullet}XeF_3$ radical is exothermic, and the binding energy of the third Xe−F bond is 8−20 kcal/mol.

1. Introduction

The recent discovery of a new type of noble-gas-containing hydrides, H−Rg−X (Rg = Ar, Kr, and Xe; X = electronegative element or group) renewed the field of rare gas chemistry and stimulated an experimental and theoretical search for novel noble-gas-containing molecules.[1−4] Most of these studies have been focused on closed-shell species, where a noble gas atom displays divalent features. Meanwhile, a series of well-known stable xenon fluorides, XeF_4 and XeF_6 (as well as xenon oxyfluorides[5,6]), demonstrates formal oxidation states of xenon of +4 and +6 that considerably broadens the range of possible xenon-containing structures (Chart 1).

The open-shell noble-gas-containing species, such as $^{\bullet}XeF_3$ and $^{\bullet}XeF_5$, attract particular interest as transient molecular structures in this series. Presently, only three neutral noble-gas-containing open-shell species, namely, $^{\bullet}XeF$,[7−9] $HXeO^{\bullet}$,[10] and $HXeCC^{\bullet}$,[11,12] were experimentally observed and characterized at experimental and theoretical levels. In the present study, we detected by FTIR spectroscopy the stabilized radical $^{\bullet}XeF_3$ in dilute mixtures of F_2 and XeF_2 in solid argon using F_2 as a photolytic precursor for fluorine atoms. We applied the obtained infrared data as a starting point for quantum-chemistry calculations to thus support our assignment for IR spectra and to rationalize the stability of chemical bonding in this radical.

2. Experimental Details

Dilute gas mixtures of F_2/Ar and XeF_2/Ar were deposited through separate stainless steel vacuum manifolds onto the golden surface of a flat cuprum finger held at 12 K in a high-vacuum chamber. The composition of typical samples was $Ar/F_2/XeF_2 = 3000:2:1$, though the relative concentrations of reactants were varied from 10^{-3} to 2×10^{-4}. The thickness of the samples was approximately 100 μm. Infrared spectra were

*To whom correspondence should be addressed. E-mail: misochko@icp.ac.ru.

(1) Khriachtchev, L.; Pettersson, M.; Runeberg, N.; Lundell, J.; Räsänen, M. *Nature* (*London*) **2000**, *406*, 874.
(2) Gerber, R. B. *Annu. Rev. Phys. Chem.* **2004**, *55*, 55.
(3) Pettersson, M.; Khriachtchev, L.; Lundell, J.; Räsänen, M. In *Inorganic Chemistry in Focus II*; Meyer, G., Naumann, D., Wesemann, L., Eds.; Wiley-VCH: New York, 2005; pp 15−34.
(4) Khriachtchev, L.; Räsänen, M.; Gerber, R. *Acc. Chem. Res.* **2009**, *42*, 183.
(5) Schumacher, G. A.; Schrobilgen, G. J. *Inorg. Chem.* **1984**, *23*, 2923.
(6) Brock, D. S.; Bilir, V.; Mercier, H. P. A.; Schrobilgen, G. J. *J. Am. Chem. Soc.* **2007**, *129*, 3598.
(7) Aquilanti, V.; Luzzatti, E.; Pirani, F.; Volpi, G. G. *J. Chem. Phys.* **1988**, *89*, 6165.
(8) Hoffman, G. J.; Colletto, M. *J. Chem. Phys.* **2001**, *114*, 2219.
(9) Misochko, E. Ya.; Akimov, A. V.; Goldshleger, I. U.; Tyurin, D. A.; Laikov, D. N. *J. Chem. Phys.* **2005**, *125*, 4503.
(10) Khriachtchev, L.; Pettersson, M.; Lundell, J.; Tanskanen, H.; Kiviniemi, T.; Runeb'erg, N.; Räsänen, M. *J. Am. Chem. Soc.* **2003**, *125*, 1454.
(11) Khriachtchev, L.; Tanskanen, H.; Lundell, J.; Pettersson, M.; Kiljunen, H.; Räsänen, M. *J. Am. Chem. Soc.* **2003**, *125*, 4696.
(12) Feldman, V. I.; Sukhov, F. F.; Orlov, A. Yu.; Tulpina, I. V.; Logacheva, E. A.; Tyurin, D. A. *Russ. Chem. Bull.* **2005**, *54*, 1458.

Chart 1

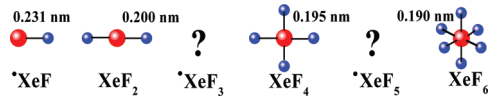

recorded with a Bruker IFS-113 V FTIR spectrometer (spectral region from 500 to 4000 cm^{-1} and spectral resolution 0.5 cm^{-1}). The closed-cycle helium refrigerator (CTI Cryogenics) was used to maintain the sample temperature in these experiments. Fluorine atoms were generated by F_2 photolysis at 337 nm with the pulse nitrogen laser. The laser light entered the sample chamber through a fused silica window and impinged on the sample at an incident angle of 45°. The beam was expanded to an area of about 4 cm^2 at the sample to ensure uniform irradiation. The average laser power was varied from 1 to 5 mW/cm^2. In some experiments, we used the second harmonic of a Nd:YAG laser (Continuum model Surelite) at 532 nm at an average laser power of 20 mW/cm^2 for photolysis of the reaction products.

To distinguish the chemical reactions involving photogenerated F atoms from those of diffusing thermal atoms, photolysis of F_2 molecules was performed at 12 K. Fluorine atoms are able to diffuse in solid argon at temperatures above 20 K.[13−15] Earlier, we used this peculiar feature of fluorine atoms to generate various novel radical species in solid argon matrices.[16] To initiate reactions of thermally diffusing F atoms, we performed annealing of photolyzed samples at temperatures above 20 K. Annealing was carried out using a step-by-step procedure. After completion of the photolysis at 12 K, the sample was annealed 2−3 min at $T > 12$ K. Then, the temperature was lowered back to 12 K, and the spectrum was recorded. This cycle was repeated 10−12 times until the reactions were complete. In a separate experiment, we verified that the 337 and 532 nm light did not induce any changes in the infrared spectra of the Ar/XeF_2 (= 3000:1) samples.

Quantum chemical calculations have been performed using three density functionals: the Perdew−Burke−Ernzerhof (PBE) nonempirical generalized gradient approximation,[17] its hybrid extension (PBE0),[18] and the popular semiempirical B3LYP model.[19] The scalar-relativistic Hamiltonian,[20] the high-quality relativistic correlation-consistent basis sets L3(F) and L33(Xe) augmented by core polarization functions,[21] and a density-fitting technique[22] as implemented in a recent version of the Priroda code[23] were used. In addition, we have tested the scalar-relativistic[20] ab initio riMP2(full) method[24] to compare with the DFT results. Molecular geometries have been fully optimized (tolerance on gradient: 10^{-5} au), and a very fine integration grid is used for the DFT exchange-correlation terms (accuracy: 10^{-8} au per atom). Unrestricted and restricted approaches have been used for calculations of the open- and closed-shell systems, respectively.

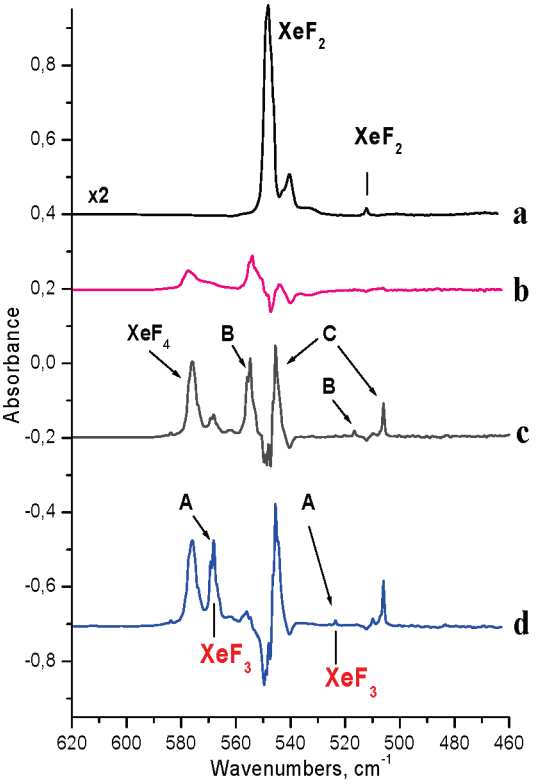

Figure 1. Infrared spectra of the $Ar/XeF_2/F_2$ (= 3000:1:2) sample at 12 K. Trace a shows IR bands of XeF_2 prior to photolysis. Trace b is the difference spectrum showing changes in the spectrum following 337 nm photolysis at 12 K. Traces c and d are the difference spectra showing additional changes occurring during short-term annealing of the sample at 27 K (c) and after subsequent prolonged annealing at 27 K (d). The IR bands labeled as **B** were assigned to the intermediate complex [XeF_2−F], and the IR bands labeled as **C** were assigned to complex [XeF_2−F_2], see text below.

3. Results and Discussion

A. Photolysis of the Samples $Ar/F_2/XeF_2$ at 12 K. The IR spectrum of the Ar/XeF_2 (= 3000:1) samples at 12 K consists of a broad band, attributed to the isolated molecules XeF_2, with a maximum at 547 cm^{-1}, which corresponds to the asymmetric stretching vibrational mode ν_3 (in an argon matrix,[25] $\nu_3 = 547$ cm^{-1}, and in a gas phase,[26] $\nu_3 = 560.1$ cm^{-1}). Additionally, a very weak band at 512 cm^{-1} is clearly seen in the spectrum that can be ascribed to the symmetric stretching vibration of XeF_2 in a matrix[27] (a corresponding IR-inactive vibration

(13) Feld, J.; Kunttu, H.; Apkarian, V. A. *J. Chem. Phys.* **1990**, *93*, 1009.
(14) Alimi, K.; Gerber, R. B.; Apkarian, V. A. *J. Chem. Phys.* **1990**, *92*, 3551.
(15) Misochko, E. Ya.; Akimov, A. V.; Wight, C. A. *Chem. Phys. Lett.* **1998**, *293*, 547.
(16) (a) Misochko, E. Ya.; Benderskii, V. A.; Goldschleger, A. U.; Akimov, A. V. *J. Am. Chem. Soc.* **1995**, *117*, 11997. (b) Misochko, E. Ya.; Akimov, A. V.; Goldschleger, A. U.; Boldyrev, A. I.; Wight, C. A. *J. Am. Chem. Soc.* **1999**, *121*, 405. (c) Misochko, E. Ya.; Akimov, A. V.; Wight, C. A. *J. Phys. Chem. A* **1999**, *103*, 7972. (d) Misochko, E. Ya.; Akimov, A. V.; Goldschleger, A. U. *Uspekhi Khim.* **2003**, *72*, 262. Misochko, E. Ya.; Akimov, A. V.; Goldschleger, A. U. *Russ. Chem. Rev.* **2003**, *72*, 233. (e) Misochko, E. Ya.; Akimov, A. V.; Belov, V. A.; Tyurin, D. A.; Laikov, D. N. *J. Chem. Phys.* **2007**, *127*, 084301.
(17) (a) Perdew, J. P.; Burke, K.; Ernzerhof, M. *Phys. Rev. Lett.* **1966**, *77*, 3865. (b) Perdew, J. P.; Ernzerhof, M.; Burke, K. *J. Chem. Phys.* **1996**, *105*, 9982.
(18) Adamo, C. *J. Chem. Phys.* **1999**, *110*, 6158.
(19) (a) Becke, A. D. *Phys. Rev. A* **1988**, *38*, 3098. (b) Lee, C.; Yang, W.; Parr, R. G. *Phys. Rev. B* **1988**, *37*, 785. (c) Becke, A. D. *J. Chem. Phys.* **1993**, *98*, 5648.
(20) Dyall, G. *J. Chem. Phys.* **1994**, *100*, 2118.
(21) Laikov, D. N. *Chem. Phys. Lett.* **2005**, *416*, 116. Electronic basis sets are designated by the symbol Λ. In the current literature, these basis sets are designated by the symbol L.
(22) Laikov, D. N. *Chem. Phys. Lett.* **1997**, *281*, 151.
(23) Laikov, D. N.; Ustinjuk, Yu. A. *Russ. Chem. Bull.* **2005**, *54*, 820.
(24) (a) Feyereisen, M.; Fitzgerald, G.; Komornicki, A. *Chem. Phys. Lett.* **1993**, *208*, 359. (b) Vahtras, O; Almlof, J. E.; Feyereisen, M. W. *Chem. Phys. Lett.* **1993**, *213*, 514.
(25) Turner, J. J.; Pimentel, G. C. In *Noble-Gas Compounds*; Hyman, H. H., Ed.; University Chicago Press: Chicago, IL, 1963; pp 101−105.
(26) (a) Agron, P. A.; Begun, G. M.; Levy, N. A.; Mason, A. A.; Jones, S. F.; Smith, D. F. *Science* **1963**, *139*, 842. (b) Burger, H.; Ma, S. *J. Mol. Spectrosc.* **1994**, *164*, 84.
(27) Howard, W. H., Jr.; Andrews, L. *J. Am. Chem. Soc.* **1974**, *96*, 7862.

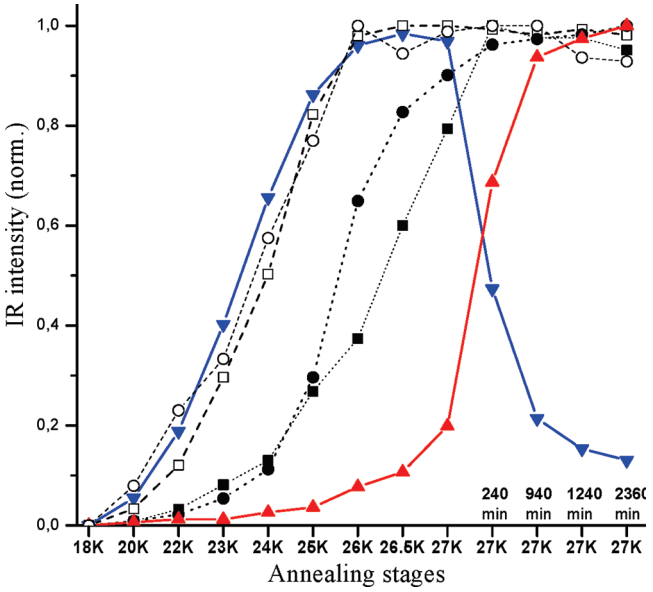

Figure 2. Consumption of the XeF_2 band at 547 cm^{-1} (○) and growth of the product bands during annealing of the photolyzed sample $Ar/XeF_2/F_2$ (= 3000:1:2): (□) FO_2 at 1489 cm^{-1}, (▼) product **B** at 554 cm^{-1}, (■) product **C** at 543 cm^{-1}, (●) XeF_4 at 576 cm^{-1}, (▲) product **A** at 568 cm^{-1}. All spectra were recorded at 12 K. The last four points show changes during annealing at 27 K.

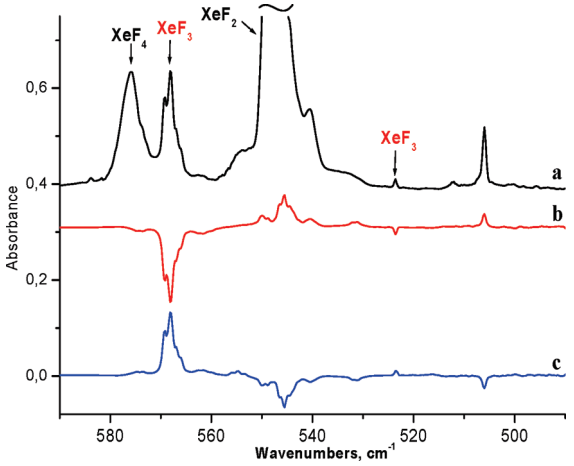

Figure 3. IR spectrum of UV-photolyzed sample $Ar/XeF_2/F_2$ (= 3000:1:2) after exhaustive annealing at 27 K (a). (b) The difference spectrum after irradiation with 532 nm light at 12 K. (c) The difference spectrum after subsequent reactions in the dark at 12 K. All spectra were recorded at 12 K.

mode of XeF_2 in a gas phase:[28] $\nu_1 = 516.5$ cm^{-1}). The IR spectrum of the $Ar/F_2/XeF_2$ (= 3000:2:1) samples at 12 K is shown in Figure 1a. It contains the same IR bands of isolated XeF_2. In addition, a red-shifted, weak broad band at 541 cm^{-1} appears in the spectrum. The intensity of this band increases with the growth of the F_2 concentration in the samples. Respectively, we assigned this band to the binary complexes $XeF_2{-}F_2$ formed upon the sample preparation.

UV-photolysis of the $Ar/F_2/XeF_2$ sample at 12 K leads to the disappearance of the IR band, attributed to the complexes $XeF_2{-}F_2$. Simultaneously, IR bands at 554 cm^{-1} (labeled with symbol **B**) and 576 cm^{-1} appear in the spectrum (see the difference spectrum in Figure 1b). The latter may be assigned to the IR-active asymmetric fundamental vibration $\nu_6(e_u)$ of the XeF_4 molecule (in a gas phase:[29] $\nu_6 = 586$ cm^{-1}). Molecules of XeF_4 can be generated in the course of a cage reaction by photolysis of the reactant complexes $[XeF_2{-}F_2]$:

$$[XeF_2{-}F_2] \xrightarrow{\lambda=337\text{nm}} [XeF_4] \qquad (1)$$

B. Annealing of the Photolyzed Samples. Annealing of the photolyzed samples leads to a decrease of the IR band at 547 cm^{-1} of isolated XeF_2 molecules. Up to 20−25% of the reactant molecules XeF_2 disappear in dark reactions upon annealing; see the difference spectra in Figure 1c and d. Simultaneously, new IR bands appear in the spectrum at 568 (labeled as **A**), 554 (**B**), 543 (**C**), 523 (**A**, very weak), 517 (**B**, very weak), 506 (**C**, weak), and 576 cm^{-1} (XeF_4). Note that IR bands labeled as **B** and **C** occur very close to fundamental absorptions of XeF_2, whereas IR bands **A** at 568 and 523 cm^{-1} are blue-shifted from $\nu_3(XeF_2)$ and $\nu_1(XeF_2)$ for 20 and 11 cm^{-1}, respectively.

The product bands demonstrate different kinetic behavior. Growth of IR bands **B**, **C**, and that attributed to XeF_4 occurs at the initial stage of annealing treatment, whereas IR band **B** disappears and growth of IR band **A** dominates upon a prolonged annealing at 27 K. Additionally, a sharp IR band at 1490 cm^{-1} of the radical FO_2 is observed in the infrared spectra of the reaction products. This radical is formed in the reaction of F atoms with O_2 molecules, as revealed in our previous reports.[15,16] Molecular oxygen is a common impurity in fluorine gas. Hence, O_2 is always present in small concentrations ($\sim 10^{-2}$ %) in samples. Since diffusing fluorine atoms react with O_2 molecules to form FO_2 radicals, we used this reaction as an internal standard for characterizing the reaction rate of diffusing F atoms (i.e., primary reactions of F atoms) upon annealing cycles. Figure 2 shows changes of IR bands at annealing cycles. Growth of the IR band at 1490 cm^{-1} reveals reactions of diffusing F atoms occurring at the temperature range from 20 to 26−27 K. Consumption of XeF_2 molecules agrees with the primary reaction of F atoms. Besides this, growth of IR band **B** corresponds to the primary reaction product at the initial stage. In contrast, growth of the band, corresponding to XeF_4 molecules, which requires two F atoms, exhibits a second-order nonlinear dependence on the concentration of primary products. Infrared bands **C** demonstrate the same kinetic behavior, justifying that product **C** requires two F atoms as well. A prolonged annealing at 27 K leads to the disappearance of IR bands **B** and the growth of IR bands **A** at 568 and 523 cm^{-1}, whereas the other product bands remain the same. This kinetic observation allows us to assume that primary product **B** corresponds to intermediate complex $XeF_2{-}F$, formed at the diffusion of fluorine atoms. Then, this complex converts to stable radical XeF_3 with a low rate at 27 K. The rate constant of the reaction

$$[XeF_2{-}F] \xrightarrow{K_r} [XeF_3] \qquad (2)$$

(28) Brassington, N. J.; Edwards, H. G. M. *J. Mol. Struct.* **1987**, *162*, 69.
(29) Claasen, H. H.; Chernick, C. L.; Malm, J. G. *J. Am. Chem. Soc.* **1963**, *85*, 1927.

Table 1. Molecular Parameters of the Series of Xenon Fluoride Compounds

	$^{\bullet}XeF$ ($C_{\infty v}$)		XeF_2 ($D_{\infty h}$)		$^{\bullet}XeF_3$ (C_{2v})	XeF_4 (D_{4h})	
	exptl[a]	calcd[b]	exptl	calcd[b]	calcd,[b] $r_1 = r_2, r_3$	exptl	calcd[b]
R(Xe−F), nm	0.231	0.234	0.200[c]	0.201	0.195, 0.226	0.192[d]	0.196
		0.231	0.198[e]	0.197	0.199, 0.223	0.195[f]	0.193
		0.237		0.200	0.197, 0.229		0.196
		0.213		0.197	0.194, 0.203		0.193
angle F−Xe−F, deg					178.6/176.6		
					178.0/178.6		
Xe−F bond dissociation energy, kcal/mol	3.4				7.5/20.0/9.0/−3.9		

[a] Data from ref 7. [b] This work: PBE0/PBE/B3LYP/MP2. [c] Data from ref 26. [d] Data from ref 31. [e] Data from ref 30. [f] Data from ref 32.

Table 2. Frequencies (cm^{-1}) of Xe−F Stretch Vibration Modes in the Series of Xenon Fluoride Compounds

	XeF_2		XeF_3		XeF_4
	ν_3 asym. stretch	ν_1 sym. stretch	ν_5 asym. stretch	ν_1 sym. stretch	ν_6 asym. stretch
calculations[a] PBE0/PBE	577.9/544.2	541.1/489.3	599.3/560.9	553.0/508.2	602.3/570.2
B3LYP/MP2	555.0/590.0	515.3/541.4	577.4/617.6	530.2/562.8	582.7/618.3
gas phase	560.1[b]	516.5[c]	579/580[d]	534/526[d]	586[e]
			581/587	533/535	
argon matrix	547[a,f]	512[a,g]	568[a]	523[a]	578
matrix shift	−13.1	−4.5	−11/−12/−13/−19	−11/−3/−10/−12	−8

[a] This work. [b] Data from ref 26. [c] Data from ref 28. [d] Predicted from calculated values and scaling factors, see text. [e] Data from ref 29. [f] Data from ref 25. [g] Data from ref 27.

is estimated as $K_r = 1/\tau \sim 7 \times 10^{-5}$ c^{-1} at 27 K, were τ is characteristic time of the dark reaction. Annealing of the photolyzed samples at different temperatures in the region of 26−30 K provides an estimate for the energy barrier of reaction 2 in an argon cage: $E \approx 1.2$ kcal/mol. On the basis of the kinetic data, the reaction product (**C**) can be assigned to complex $[XeF_2-F_2]$ resulting from the reaction of diffusing fluorine atoms with the primary product **B**:

$$[XeF_2-F] + F \xrightarrow{K_F} [XeF_2-F_2] \quad (3)$$

Hence, the IR bands (**C**) occur very close to the IR bands of reactant complex $[XeF_2-F_2]$ formed during sample preparation. The secondary reaction of diffusing F atoms is the main source of XeF_4 molecules, the formation of which being clearly observed in spectra of the products. According to the proposed scheme, XeF_4 is formed in the course of the reaction of mobile fluorine atoms with XeF_3:

$$[XeF_3] + F \xrightarrow{K_F} [XeF_4] \quad (4)$$

C. Photolysis of the Reaction Products with Laser Light at 532 and 337 nm. To test the photostability of the reaction products in visible and UV light, a sample containing the reaction products was subjected to irradiation by 532 and 377 nm laser light. Figure 3 shows changes in the spectrum after photolysis with 532 nm green light at 12 K. Photolysis results in the disappearance of two product bands (**A**) at 568 and 523 cm^{-1}. Simultaneously, growth of the bands at 545 and 504 cm^{-1} takes place. These bands disappear in the subsequent dark reaction with a characteristic time of about 100 min at 12 K, and IR bands at 568 and 523 cm^{-1} recover up to 80−90% of the starting intensities (i.e., before the green light irradiation). So, this experiment demonstrates decomposition of XeF_3 by means of green-light photolysis, whereas a formed intermediate product with IR bands at 545 and 504 cm^{-1} is highly unstable, even at 12 K. If irradiation by green light is performed at 18 K, then the intermediate complex decays in the dark with a characteristic time of about 3−5 min.

In the next experiment, the same sample was exposed to the irradiation with light at 337 nm. Photolysis leads to the consumption of bands (**C**) at 543 and 506 cm^{-1} and predominant growth of the IR band at 578 cm^{-1} assigned to the XeF_4 molecule, as well as to growth of IR bands (**A**) at 568 and 523 cm^{-1}, which we have assigned to radical XeF_3. In the frame of our assignments of IR product bands, UV photolysis of the secondary product (complexes **C**) creates two reaction channels:

$$[XeF_2—F_2] \xrightarrow{\lambda=337\,nm} \begin{matrix} \nearrow [XeF_4] \\ \searrow [XeF_3] + F_{stab}. \end{matrix} \quad (5)$$

where [...] means a solid argon cage and F_{stab} stands for a stabilized fluorine atom outside of a parent cage.

D. Quantum-Chemical Calculations of Radical XeF_3. We carried out quantum-chemical calculations to support our assignments for the infrared spectrum of radical XeF_3. We have calculated four molecular structures of $^{\bullet}XeF$, XeF_2, $^{\bullet}XeF_3$, and XeF_4 to compare our calculation results with available experimental data. Table 1 provides the obtained molecular parameters for these species. It shows that the calculated distances Xe−F in XeF_2 and XeF_4 agree well with the experimental data. Practically, the same distance is calculated for symmetric fragment F−Xe−F in the $^{\bullet}XeF_3$ radical. Calculations predict that radical $^{\bullet}XeF_3$ corresponds to the C_{2v} point group with a F−Xe−F angle of 176−178°. Calculations show a much

Table 3. Calculated vibrational frequencies of the radical XeF_3

			calculated harmonic frequencies, cm^{-1}			
vib. sym.	no	approximate type of mode	PBE0	PBE	B3LYP	MP2
a_1	ν_1	sym XeF_2 stretch	555.3	506.2	530.2	562.8
	ν_2	XeF(3) stretch	254.9	308.3	250.3	424.6
	ν_3	XeF_2 in-plane bend	195.8	169.2	189.7	195.6
b_1	ν_4	out-of-plane bend	220.2	202.5	212.3	224.9
b_2	ν_5	asym. XeF_2 stretch	599.3	560.9	577.4	617.6
	ν_6	FXeF(3) bend (in-plane)	79.3	68.4	80.13	101.8

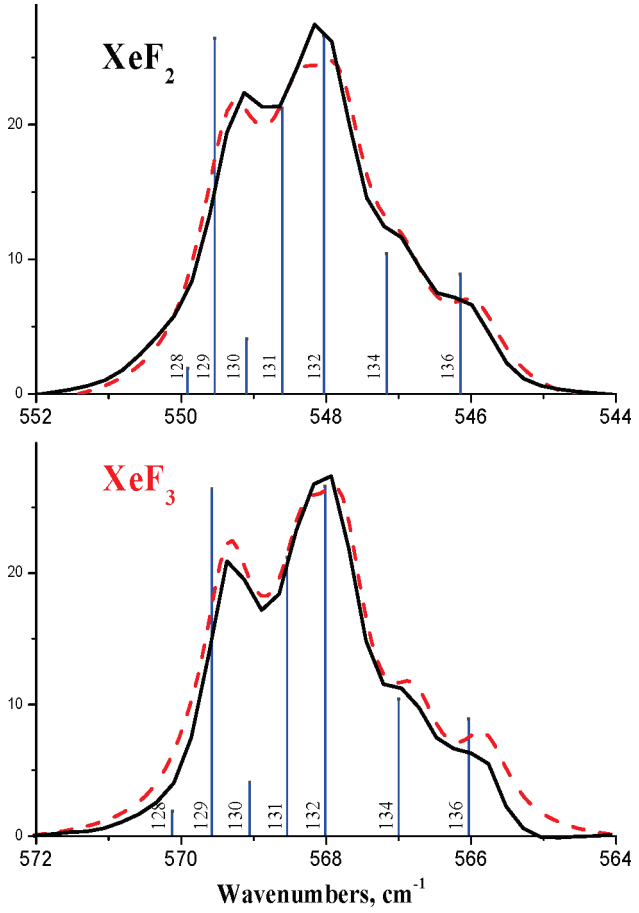

Figure 4. IR absorption of IR-active mode in solid argon matrices recorded at 12 K with spectral resolution of 0.5 cm^{-1}, dark lines. Dashed lines are the simulated spectra based on PBE0-calculated vibrational frequencies of the ν_3 mode for different xenon isotopomers XeF_2 and the ν_5 mode for XeF_3 (vertical sticks), scaled with eq 5. The Lorenzian shape of the lines with a line width of $\delta = 0.85$ cm^{-1} was applied. The height of vertical sticks shows the abundance of xenon isotopes in naturally occurring xenon (in percent).

shorter distance for Xe−F in the $^{\bullet}XeF_3$ radical rather than that in $^{\bullet}XeF$.

Calculated harmonic vibrational frequencies of XeF_2, XeF_3, and XeF_4 are shown in Table 2 in comparison with the experimental data. These molecules have one IR-active vibration only in our experimental region, where $\nu > 500$ cm^{-1}. Thus, we assign a strong IR band at 568 cm^{-1} to the asymmetric stretching vibrational mode ν_5 of $^{\bullet}XeF_3$. A very weak band at 523 cm^{-1} (see Figure 1d and Figure 3b) can be attributed to the symmetric stretch vibration ν_1 in a solid matrix. The other calculated fundamental vibrations of XeF_3 are presented in Table 3. The calculated harmonic vibrational frequencies differ by only 1−5% from those experimentally observed in the gas phase for $\nu_1(XeF_2)$, $\nu_3(XeF_2)$, and $\nu_6(XeF_4)$. Better agreement between theoretical and experimental IR data for closed-shell species is obtained by using the B3LYP functional. Calculations by this method overestimate the corresponding frequencies in the gas phase by factors of 1.009, 1.002, and 1.006, respectively (the average scaling factor $k = 1.006$). The other methods yield the average scaling factors k(PBE0) = 0.966, k(PBE) = 1.034, and k(MP2) = 0.95. We have used these scaling factors to estimate the gas-phase values and matrix shifts for vibrational frequencies ν_1 and ν_5 in the radical $^{\bullet}XeF_3$, see Table 2. IR-active modes are red-shifted in a matrix: $\Delta\nu_3 = -12$ cm^{-1} in XeF_2, $\Delta\nu_1 = (-11$ to $-19)$ cm^{-1} in $^{\bullet}XeF_3$, and $\Delta\nu_6 = -8$ cm^{-1} in XeF_4. The vibration mode ν_1 has a small matrix shift: $\Delta\nu_1 = -4.5$ cm^{-1} in XeF_2 and $\Delta\nu_1 = (-3$ to $+10)$ cm^{-1} in $^{\bullet}XeF_3$.

In our measurements, we used naturally occurred xenon, containing various xenon isotopes. The next series of calculations was to obtain the vibrational frequencies of XeF_2 and $^{\bullet}XeF_3$ for different isotopes: ^{128}Xe, ^{129}Xe, ^{130}Xe, ^{131}Xe, ^{132}Xe, ^{134}Xe, and ^{136}Xe. Using the above estimated scaling factors and matrix shifts for the IR-active mode, we calculated frequencies for each isotopomer in a matrix:

$$\nu(\text{matrix}) = \nu(\text{calcd}) \times 0.966 + \Delta\nu \qquad (5)$$

Figure 4 shows the simulated IR bands ν_3 for XeF_2 and ν_5 for $^{\bullet}XeF_3$ in comparison with those experimentally registered at 12 K. This demonstrates that the calculated spectra reproduce broad experimental bands in accordance with the natural abundance of xenon isotopes. To the contrary, the calculated frequencies of symmetric stretch mode ν_1 are not sensitive to xenon isotopes, as was expected for such a type of vibration. Thus, both IR bands ν_1 at 512 (XeF_2) and 523 cm^{-1} (XeF_3) are narrow in experimental spectra (line width ≤ 2 cm^{-1}).

We also calculated the strength of the third Xe−F(3) bond in radical $^{\bullet}XeF_3$. The DFT calculations indicate that $^{\bullet}XeF_3$ in the gas phase is stable toward dissociation of the Xe−F(3) bond, see Table 1. Our estimation predicts thermal stability of the radical $^{\bullet}XeF_3$ at cryogenic temperatures and exothermicity of the addition of the fluorine atom to the XeF_2 molecule. Also, it reveals that the strength of the Xe−F(3) bond in the $^{\bullet}XeF_3$ radical should be higher than that in the $^{\bullet}XeF$ radical. In contrast, the MP2 calculation predicts endothermicity for the addition of the F atom to the XeF_2 molecule and, subsequently, a very high reaction barrier, $E > 3.9$ kcal/mol.

(30) Reichman, S.; Schreiner, F. *J. Chem. Phys.* **1969**, *51*, 2355.
(31) Ibers, J A.; Hamilton, W. C. *Science* **1963**, *139*, 106.
(32) Burns, J. H.; Agron, P. A.; Levy, N. A. In *Noble-Gas Compounds*; Hyman, H. H., Ed.; University Chicago Press: Chicago, IL, 1963; p 211.

4. Conclusions

The main experimental result of the present study is that the reaction $F + XeF_2$ in solid argon produces new radical species $^{\bullet}XeF_3$. Kinetic and spectroscopic observations in combination with calculated vibrational frequencies of a series of xenon fluoride compounds justify this conclusion. The formation of radical $^{\bullet}XeF_3$ obeys specific kinetic behavior indicating the formation of a long-lived intermediate complex under the condition that the diffusing fluorine atom is attached to isolated XeF_2 at temperatures 20 K $< T <$ 27 K. Subsequent thermally activated conversion (eq 2) of this complex is the main source of new radical species. At this stage, we cannot make a definite conclusion about the origin of the energy barrier for this reaction. Nevertheless, the disappearance of radical $^{\bullet}XeF_3$ upon the green-light irradiation and the fast recoverability in the dark at 12 K (Figure 3) suggest that a solid-argon cage assists in the formation of an intermediate prereaction complex and, subsequently, provides an effective reaction barrier, which depends on the experimental conditions. On the basis of this fact, we assume that the energy barrier for this reaction in the gas phase should be lower by 1 kcal/mol. We believe that these data could serve as a starting point for more accurate and detailed quantum-chemical calculations aimed at the understanding of the electronic structure and chemical properties of this intermediate. Ab initio calculations and experimental studies, employing the radical $^{\bullet}XeF_3$ as a precursor in the synthesis of novel closed-shell noble-gas compounds, are now being carried out.

Acknowledgment. This research is supported by INTAS (Grant No. 05-1000008-8017) and the Russian Foundation for Basic Research (Grant No. 07-03-00768). We thank Dr. D. Laikov for use of his software "Priroda" and useful advice about calculations. We thank the Russian Academy of Sciences Joint Supercomputer Center for computational resources.